Available online at www.sciencedirect.com
ScienceDirect
Journal of the European Ceramic Society 27 (2007) 673–678
www.elsevier.com/locate/jeurceramsoc

Tape casting of new electrolyte and anode materials for SOFCs operated at intermediate temperature

S. Beaudet Savignat*, M. Chiron, C. Barthet

CEA Le Ripault, Département Matériaux, BP 16, 37260 MONTS, France

Available online 5 June 2006

Abstract

An important task in SOFC research is the reduction of the operating temperature to 700 °C, to avoid premature ageing of the cell components and the use of expensive interconnect materials. This requires the development of new electrolytes and electrodes materials.

Oxyapatite electrolytes have recently attracted considerable attention and we have already reported some interesting performances for the $La_9Sr_1Si_6O_{26.5}$ composition ($\sigma = 8.8 \times 10^{-3}$ S cm^{-1} at 700 °C) [Beaudet Savignat, S., Lima, A., Barthet, C. and Henry, A., In *Proceedings of the International Symposium Solide Oxide Fuel Cells VIII, Vol. 2003–2007*, pp. 372–378].

This study was centered on the manufacturing of an apatite electrolyte and a Ni/apatite cermet anode by the tape casting process, with a view to the development of anode/electrolyte 1/2 cells.

Slurries compositions were first optimized to adjust green tapes characteristics. Secondly, we focused on the binder burnout and the sintering. Dense electrolytes were synthesized. The influence of the particle size of the apatite powder, with a fixed NiO powder particle size, and the influence of the addition of pyrolyzable organic particles on the sintering and the microstructure of the anode material were studied.

Keywords: Fuel cells; Tape casting; Apatite; Microstructure-final; Co-sintering

1. Introduction

One of the most important tasks in SOFC research is the reduction of operating temperature from 900–1000 °C down to 700–800 °C, to avoid premature ageing of the cell components and the use of expensive interconnect materials. This requires extremely thin YSZ electrolytes or the development of new electrolytes and electrodes materials with good performances between 700 and 800 °C.

Rare earth based apatites are viable electrolyte materials for Intermediate Temperature SOFCs with their open crystalline structure including channels for the diffusion of oxide ions and the well known chemical stability of the apatite structure. We have previously reported interesting performances for the $La_9Sr_1Si_6O_{26.5}$ apatite composition[1], with a conductivity of 8.8×10^{-3} S cm^{-1} at 700 °C and an activation energy of 0.8 eV, lower than that of YSZ.[2,3]

New electrodes materials are also developed. A Ni/$La_9Sr_1Si_6O_{26.5}$ apatite cermet was chosen in this study for the anode. The proper characteristics for this material are a good chemical stability, an expansion coefficient compatible with the other cell components, a good adhesion to the electrolyte material, 20% of open porosity before the reduction of NiO to Ni and 30–40% of open porosity after reduction for efficient gas transportation, and a sufficient nickel content to insure a good electronic conductivity.

A planar electrolyte supported SOFC is an attractive geometry for a stack configuration. Relatively large and flat cell components are required for such designs. The tape casting process is a reliable, cost effective manufacturing technique, widely used in the microelectronics industry. Therefore, it was chosen in this work to develop electrolyte/anode 1/2 cells.

We first optimized the compositions of the electrolyte and anode slurries to obtain green tapes with suitable characteristics in terms of thickness, density, mechanical resistance and homogeneity. In a second part, we focused on the binder burnout and the sintering. We optimized the heat treatment parameters to obtain dense and flat electrolyte samples with a thickness of 150–200 μm and then we studied the co-sintering of an electrolyte/anode 1/2 cell. To adjust the sintering behaviour of the two materials and the microstructure of the anode (porosity and Ni distribution), we investigated the influence of the particle size

* Corresponding author. Tel.: +33 47 34 48 52; fax: +33 2 47 34 51 83.
E-mail address: sophie.beaudet-savignat@cea.fr (S. Beaudet Savignat).

0955-2219/$ – see front matter © 2006 Elsevier Ltd. All rights reserved.
doi:10.1016/j.jeurceramsoc.2006.04.049

of the apatite powder, with a fixed NiO powder particle size, and the addition of pyrolyzable organic particles.

2. Experimental

2.1. Powder processing

The $La_9Sr_1Si_6O_{26.5}$ electrolyte powder was prepared by solid-state reaction. High purity oxides (La_2O_3, SiO_2) and carbonates ($SrCO_3$) were ball milled in ethanol for 24 h in plastic vessels. The dried powder was subsequently calcined in air at 1500 °C. A wet attrition milling or a dry grinding was performed to reduce the powder particle size. The final powder exhibits a mean particle diameter of 1.1 μm for the attrition milling and 3 μm for the dry grinding, according to laser grain size analysis. Some SEM images of the powders are also shown on Fig. 1. A commercial NiO black powder (Inco) was chosen for the elaboration of the cermet. This powder is strongly agglomerated with a crystallite size between 0.1 and 0.6 μm. It was ball milled in ethanol for 24 h to reduce the mean particle diameter down to 1 μm. The apatite and NiO powders were finally ball milled in ethanol for 24 h to obtain the cermet powders. The NiO content was chosen to obtain a Ni content of 40 vol% after reduction. The cermet powders compositions and grain sizes are shown in Table 1. The cermets with the 1.1 and 3 μm apatite powder are referred to as respectively CERM1/1 and CERM1/3.

2.2. Tape casting process

The first stage in the tape casting process involves dispersing the ceramic powders in a solvent with the addition of binders and plasticizers to yield the proper slip rheology.

The solvent used is an azeotrope of 66% MEK—34% ethanol.

Table 1
Compositions and grain sizes of the cermet powders

Powder	Composition (Ni vol%/apatite vol%)	NiO grain size (μm)	Apatite grain size (μm)
CERM1/1	40/60	1	1.1
CERM1/3			3

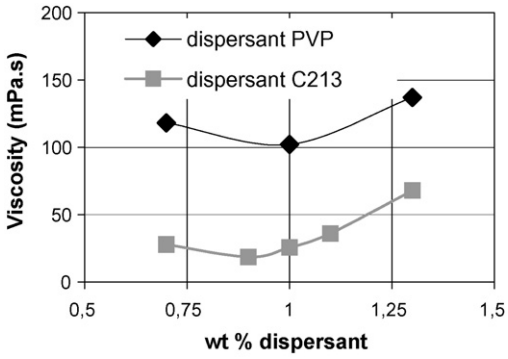

Fig. 2. Optimization of the dispersant content for the electrolyte slip.

The dispersant nature and content are optimized by rheology measurements using a Brookfield III viscosimeter. Two dispersants were chosen for the dispersion of the electrolyte slip: a phosphate ester (Beycostat C213) and polyvinylpyrrolidone (PVP). The powder, the solvent and the dispersant were ball milled for 24 h before viscosity control. The evolution of the electrolyte slip viscosity at 30 s^{-1} versus the dispersant content (in wt.% of the total amount of mineral powder) is shown on Fig. 2. The lowest viscosity was observed for 0.9 wt.% of C213 dispersant. Stabilization of the dispersion for this dispersant is brought about by two mechanisms: steric hindrance and electrostatic repulsion,[4] whereas a single steric hindrance mechanism is reported for PVP.[5] The same study was performed for CERM1/1 and CERM1/3 with the dispersant C213 only. The lowest viscosity was observed for 1.2 and 1.1 wt.% of C213 dispersant respectively for CERM1/1 and CERM1/3. A higher dispersant content was required for the cermet powder of finer particle size.

The binder and plasticizer contents are optimized according to the slip viscosity and the green tapes properties.

To adjust the sintering behaviors of the electrolyte and the cermet and to increase the porosity of the cermet before reduction, we studied the influence of the addition of pore-forming agents (PFAs). These PFAs are introduced during the slip preparation and removed during binder burnout, leaving stable voids that are not destroyed during the subsequent sintering step. This method offers several advantages: the possibility to control the porosity characteristics (volume fraction, size and shape) and hence to adjust the anode electrochemical performances and to

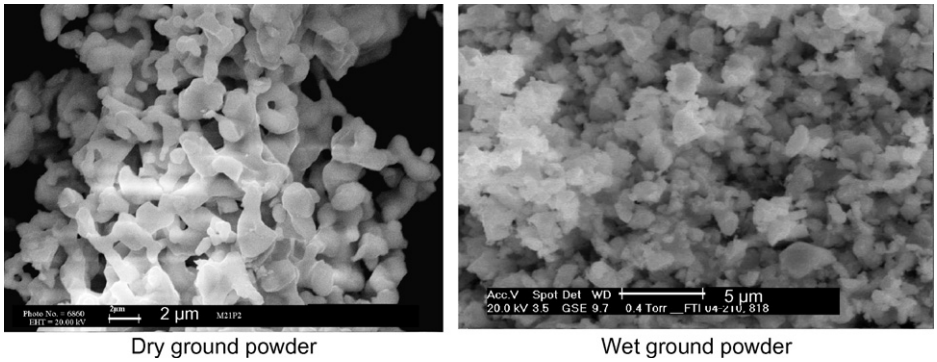

Fig. 1. Microstructure of the electrolyte powders.

suppress the differential sintering between electrolyte and anode materials. We selected a graphite and a starch powder with surface areas of respectively 13.6 and 0.36 m^2/g and very different particle shapes (Fig. 5). The slips compositions were adjusted according to the method of weight compensation of Corbin et al.[6] (the weight ratio between organics and total powder (cermet + PFA) was kept constant).

The slurries were cast using a moving single blade/stationary mylar film carrier machine. The blade height was adjusted to obtain green tapes with a thickness of 200 μm for the electrolyte and 50 μm for the anode.

Green densities and thicknesses were controlled after drying on punched tape pellets.

Sintered bulk porosity was controlled by the Archimedes method and pore size distribution by Hg intrusion. As the sintered tapes were too fragile, these measurements were performed on massive pellets of several millimeters height obtained by lamination of several punched tape pellets under 150 MPa at 100 °C. Dilatometry samples were prepared in the same way for experiments in air (Setaram dilatometer TMA92).

3. Results

3.1. Optimization of the binder and plasticizer contents

The next step was the addition of an acrylic binder (Degalan LP 51–07) and a phthalate plasticizer (DBP). Electrolyte slips were produced with a binder content between 4 and 6 wt.% and a plasticizer content between 4 and 7 wt.%. The observations made on the green tapes are presented in Table 2. Formulations A and B led to tapes with optimum properties: good removal from carrier surface, no cracking, high green density, good microstructural homogeneity (see Fig. 3), reproducible thickness. To minimize the organics content in the tapes, we retained formulation A.

For the cermet powders, a binder content of 5 wt.% and a plasticizer content of 8 wt.% were optimized in the same way.

3.2. Sintering

3.2.1. Preliminary dilatometric study

For a co-sintering of 1/2 cells, it is necessary to adjust the sintering of both materials. The sintering behaviour of the two base materials, electrolyte and NiO, and of the two cermets was studied by dilatometry under air during heating up to 1600 °C (see Fig. 4).

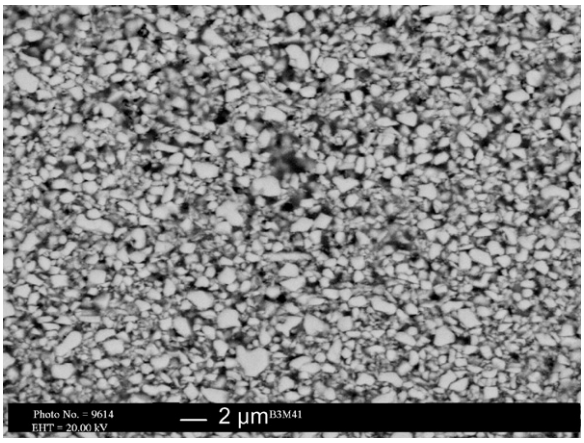

Fig. 3. SEM image of an electrolyte green tape of formulation A.

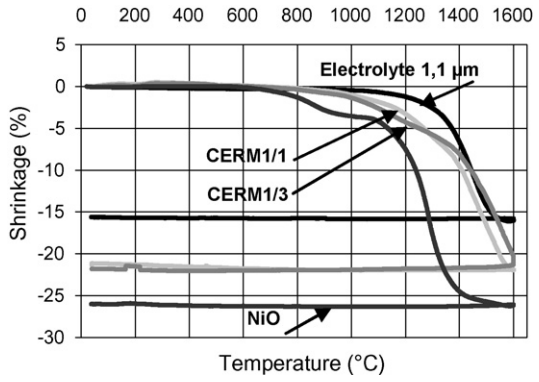

Fig. 4. Dilatometric curves of tapes of electrolyte, CERM1/1, CERM1/3 and NiO.

The sintering rates of the base materials, apatite and NiO, are very different. The sintering of NiO is activated at low temperature (~500 °C) with a great overall shrinkage; this behavior is in good agreement with the high surface area measured by the BET gas absorption method for this powder (73.5 m^2/g). The sintering of the apatite electrolyte is activated at high temperature (>1100 °C for the 1.1 μm powder, >1200 °C for the 3 μm powder, not included on Fig. 4) with a moderate shrinkage. The sintering behaviors of the cermets fall between those of the two base materials and are not compatible with the electrolyte. In the case of a 1/2 cell co-sintering, the sintering temperature will be

Table 2
Properties of electrolyte green tapes

Reference of the formulation	Binder (wt.%)	Plasticizer (wt.%)	Thickness (μm)	Observations	Apparent green density ($g\,cm^{-3}$)
A	5	5	187 ± 5	No defects	2.88 ± 0.01
B	5	6	214 ± 5	No defects	2.88 ± 0.02
C	6	6	176 ± 5	Cracks	2.84 ± 0.03
D	4	4	207 ± 5	Difficult tape removal	–
E	4	5	196 ± 5	Difficult tape removal	–
F	4	6	213 ± 5	Difficult tape removal	–
G	4	7	202 ± 5	Difficult tape removal	–

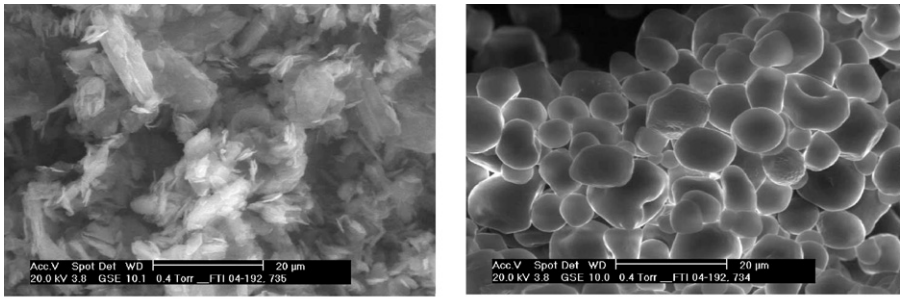

Fig. 5. Microstructure of the PFAs powders.

imposed by the electrolyte, with a required final density of 95% of theoretical, to prevent gas cross leakage.

3.2.2. Electrolyte sintering

Tapes samples of formulation A were heated under air in two stages: a binder burnout stage (30 °C/h up to 500 °C) to allow the organics combustion, according to a thermogravimetric analysis, and a sintering stage (150 °C/h up to 1550 °C). Table 3 presents the sintered densities, as well as the thicknesses of sintered samples. The influence of a lamination at 150 MPa, 100 °C, and of the sintering dwell time were also studied. We see that the green and sintered densities increase slightly with the number of layers and, in the case of a single layer, with a lamination. The increase of the sintering dwell time from 2 to 4 h improves the sintered densities, with a good value of 94.9% for a single layer. However, all sintered samples present significant deformations. A pressure assisted sintering with very small loads and a reduction of the binder burnout rate from 30 to 10 °C/h minimize these deformations.

3.2.3. Anode sintering

The heat treatment parameters optimized for the electrolyte were applied to the anode material. Flat CERM1/1 and CERM1/3 samples were successfully obtained. However, as expected from the dilatometric experiments, the high densities measured on these samples (97.8 and 98.3% of theoretical respectively for CERM1/1 and CERM1/3) are not compatible with our objective of 20% of open porosity before reduction.

3.2.4. Co-sintering of 1/2 cells

Some electrolyte/anode 1/2 cells (electrolyte diameter: 38 mm, anode diameter: 32 mm) were successfully manufactured by co-tape casting. A co-sintering was performed under air with the precedent parameters. The resulting samples were cracked, distorted, with delaminations between the two materials. A lamination did not improve these results.

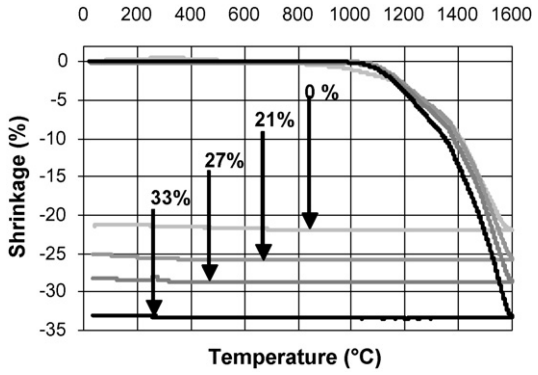

Fig. 6. Dilatometric curves of tapes of CERM1/1 with and without graphite addition.

3.2.5. Addition of pore forming agents to the anode

3.2.5.1. Graphite addition. The dilatometric behavior of CERM1/1 tapes with different graphite contents between 0 and 33 vol% is shown on Fig. 6. The sintering shrinkage increases with the graphite content. We also observe an increase in the initial sintering temperature for all tapes with graphite addition. These tapes were previously debound at 1000 °C to remove the organics and the graphite and to avoid significant disturbances of the dilatometric experiments. However, the first stage of sintering is already activated at 1000 °C for the cermet powder (see Fig. 4), which could explain these higher initial sintering temperatures.

Another important sintering characteristic to consider is the sintered bulk porosity measured on laminated samples of a

Table 3
Properties of electrolyte sintered samples

Sample reference	Number of layers	Lamination	Sintering	Sintered density (g/cm^3) (% of theoretical density)	Thickness (μm)
A-1	1	No	1550 °C 2 h	5.03 (92.1%)	190
A-2	1	Yes	1550 °C 2 h	5.06 (92.7%)	170
A-3	1	Yes	1550 °C 4 h	5.18 (94.9%)	170
A-4	2	Yes	1550 °C 2 h	5.17 (94.7%)	340
A-5	2	Yes	1550 °C 4 h	5.28 (96.6%)	340

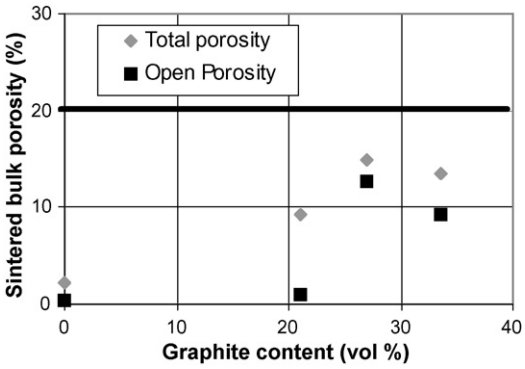

Fig. 7. Bulk porosity versus graphite content for CERM1/1 sintered under air at 1550 °C 4 h.

few millimeters thickness (Fig. 7). The porosity level increases with the graphite content up to 27 vol% and decreases beyond; it remains smaller than our objective of 20% after air sintering, in all cases. The open porosity level is very low for a 21 vol% graphite content and increases suddenly for a 27 vol% graphite content, which may be related to a percolation threshold. The porosity created by graphite addition is apparently not stable. The high BET surface area and the strong morphological anisotropy of the graphite powder (plate-like shape) may explain this instability during the sintering step.

The same study was performed for CERM1/3. A graphite content of 21 vol% was tested in the first place. Same modification of the sintering behavior is observed with the PFA addition as for CERM1/1. The porosity level measured on a sample sintered at 1550 °C for 4 h was consistent with our objective of 20% (Fig. 8 before reduction); an average pore diameter of 0.8 μm was measured by Hg intrusion. We next studied the reduction of NiO to Ni by thermogravimetric analysis. The reduction is complete after 5 h at 900 °C, with a total weight loss of 12.9% in good agreement with the theoretical value of 12.6% for a composition of 40 vol% Ni and 60 vol% apatite. The porosity measurements performed on reduced samples revealed a final porosity level in good agreement with our objective of 30% (Fig. 8 after reduction). An optical micrography of a reduced sample (Fig. 9) reveals a homogeneous distribution of the porosity (in black) and the Ni (in white). An increase in the average

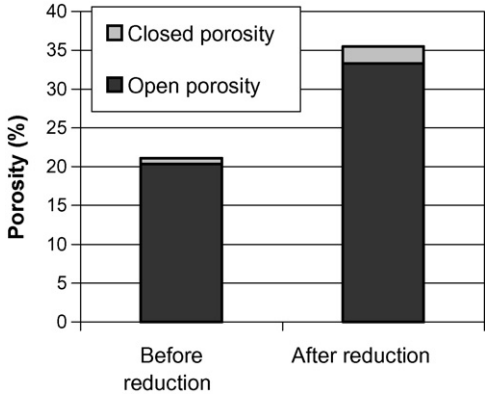

Fig. 8. Sintered bulk porosity before and after reduction for CERM1/3 with 21 vol% graphite.

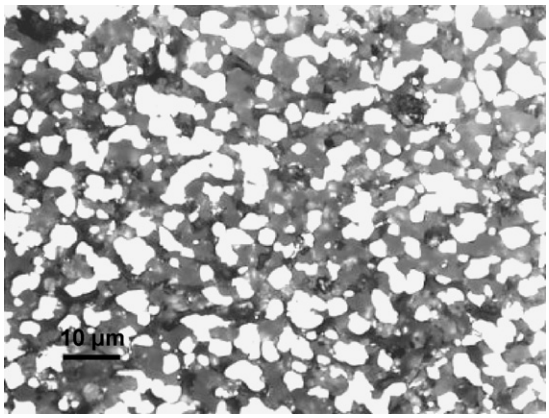

Fig. 9. Optical micrography of a reduced CERM1/3 sample with 21 vol% graphite.

Table 4
Comparison of sintering shrinkages at 1550 °C for graphite and starch additions

PFA addition	PFA content (vol%)	Sintering shrinkage at 1550 °C (%)
No PFA	0	16.7
Starch	25.5	19.8
Graphite	21	24.4

pore size was noticed by Hg intrusion, from 0.8 μm for the air sintered sample to 1.6 μm for the reduced sample. This low value after reduction is consistent with our previous speculation that the average particle size of the graphite powder is to small to leave stable pores in the anode. We will therefore now present our results for the starch addition. We expect a greater stability for this PFA, on account of its greater particle size and its spherical particle shape.

3.2.5.2. Starch addition. 25.5 vol% starch was added to CERM1/3. The sintering shrinkage of the cermet increases with starch addition, as it does with graphite. If we compare the sintering shrinkages at the electrolyte sintering temperature (1550 °C) (Table 4), a 25.5 vol% starch addition seems more favorable than a 21 vol% graphite addition. The evolution of the sintered porosity with the starch content in the cermet is shown on Fig. 10. The porosity level increases with the starch content up to 19 vol% and

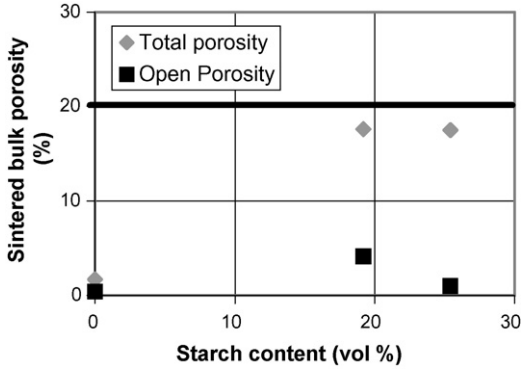

Fig. 10. Bulk porosity versus starch content for CERM1/3 sintered under air at 1550 °C 4 h.

remains steady beyond. This porosity mainly consists of closed porosity and is not stable during the sintering stage. The average pore diameter of 0.8 μm measured by Hg intrusion is similar to the one previously observed for CERM1/3 with graphite addition. We suppose that the lamination pressure (150 MPa) was too high and deformed the PFAs particles.

4. Conclusion

Tape casting of apatite electrolyte and Ni/apatite anode was successfully performed. The sintering parameters of the electrolyte tapes were optimized to obtain dense samples with a suitable thickness and a good flatness. Same parameters applied to the anode lead to flat samples with insufficient porosity levels. The anode tapes exhibit enhanced shrinkage and reduced sintering temperature compared to the electrolyte. The co-sintering of 1/2 cells therefore leads to cracking, deformations and delaminations. The graphite addition increases the porosity level of the anode but also the sintering shrinkage. The porosity levels remain however insufficient for the anode with the finest apatite powder. For the anode with the coarser apatite powder, the porosity levels fit with our objectives and the Ni distribution is homogeneous. Starch addition also increases the sintering shrinkage and leads to insufficient porosity levels in air sintered samples, whatever the PFA's content. Further investigations will be performed to confirm and improve these results by reducing the lamination pressure before sintering to avoid deformation of the PFAs particles, by adjusting the green densities of the tapes or by testing a coarser NiO powder and a finer apatite electrolyte powder in order to reduce the sintering mismatch between the electrolyte and the cermet.

References

1. Beaudet Savignat, S., Lima, A., Barthet, C. and Henry, A., In Proceedings of the International Symposium Solide Oxide Fuel Cells VIII, Vol. 2003–2007, 2003, pp. 372–378.
2. Lee, C. H. and Choi, G. M., Electrical conductivity of CeO_2-doped YSZ. *Solid State Ionics*, 2000, **135**, 653–661.
3. Kim, J. H. and Choi, G. M., Mixed ionic and electronic conductivity of $[(ZrO_2)_{0.92}(Y_2O_3)_{0.08}]_{1-y}(MnO_{1.5})_y$. *Solid State Ionics*, 2000, **130**, 157–168.
4. Mikeska, K. and Cannon, W. R., Non aqueous dispersion properties of pure barium titanate for tape casting. *Colloids Surf.*, 1988, **29**, 305–321.
5. Esumi, K., Takamine, K., Ono, M. *et al.*, The interaction of poly(vinylpyrrolidone) and solid particles in ethanol. *J. Colloid Interface Sci.*, 1993, **161**, 321–324.
6. Corbin, S. F. and Apté, P. S., Engineered porosity via tape casting, lamination and the percolation of pyrolyzable particulates. *J. Am. Ceram. Soc.*, 1999, **82**(7), 1693–1701.